ACS APPLIED POLYMER MATERIALS

pubs.acs.org/acsapm Article

Ether-free Poly(arylene methylimidazole) Membranes with High Performance for Vanadium Redox Flow Battery Applications

Meichen Zhang,[§] Peiru Lv,[§] Lele Wang, Jin Wang,* and Jingshuai Yang*

Cite This: https://doi.org/10.1021/acsapm.4c03945 Read Online

ACCESS | Metrics & More | Article Recommendations | Supporting Information

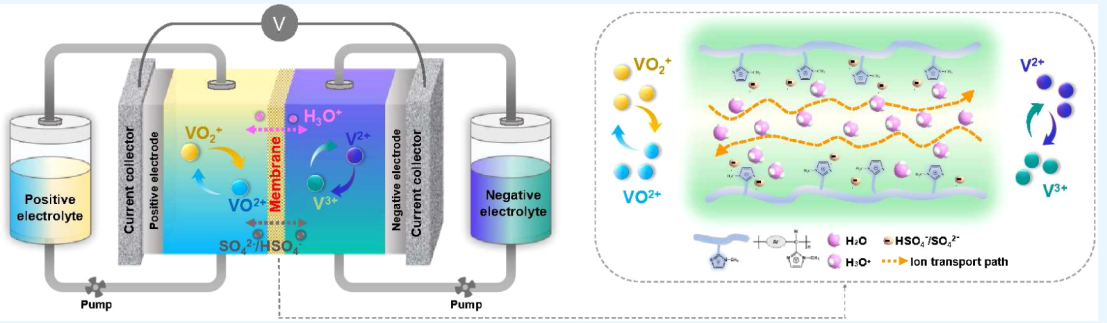

ABSTRACT: Achieving superior ionic selectivity in membranes is vital for enhancing the performance of vanadium redox flow batteries (VRFBs). In this study, we synthesize a series of ether-free poly(arylene methylimidazole) copolymers (P(MeIm-*co*-*X*)) enriched with methylimidazole groups. These copolymers are prepared via a straightforward superacid-catalyzed polymerization of 1-methyl-2-imidazolecarboxaldehyde with five distinct aromatic monomers: biphenyl, fluorene, 1,2-diphenylethane, diphenyl sulfide, and *p*-terphenyl (used as a reference). Our objective is to investigate how variations in the polymer backbone's chemical structure affect membrane properties relevant to VRFB applications. The incorporated basic methylimidazole groups facilitate ion transport through hydrogen bonding, while modifications in the aromatic monomer structures adjust the polymer microstructure to optimize area resistance and ionic selectivity. Among the synthesized membranes, the fluorene-based P(MeIm-*co*-Flu) exhibits the most outstanding performance, displaying excellent chemical stability, high tensile strength (22.4 MPa), and low area resistance (0.32 Ω cm^2). When evaluated in VRFBs at a current density of 100 mA cm^{-2}, the P(MeIm-*co*-Flu) membrane achieves an energy efficiency (EE) of 85.7%, surpassing that of Nafion 115 (76.5%). Additionally, this membrane demonstrates exceptional capacity retention over 570 cycles at 100 mA cm^{-2}, maintaining Coulombic efficiencies above 99%, with energy efficiencies decreasing slightly from 85.4% to 80.9%. Therefore, this work presents a high-performance, easily synthesized, and cost-effective P(MeIm-*co*-Flu) membrane for potential application in VRFBs.

KEYWORDS: *polymer membrane, poly(arylene methylimidazole), ionic selectivity, energy efficiency, vanadium redox flow battery*

1. INTRODUCTION

As global efforts intensify to reduce carbon emissions, sustainable clean energy sources like wind and solar power are increasingly favored.[1] However, due to the unpredictable availability of these energy sources, developing high-performance energy storage systems is crucial.[2,3] Among these, vanadium redox flow batteries (VRFBs) are regarded as particularly promising. By leveraging the multivalence of vanadium ions, VRFBs offer stable output power, and long operational lifespans, and are gradually being implemented in practice.[4,5−7] A crucial component of VRFBs is the separator membrane, which not only prevents cross-contamination between vanadium ions of different valence states but also facilitates rapid proton transport to complete the circuit,[5,8,9] Therefore, an optimal membrane material should offer robust resistance to vanadium ion permeation, exhibit high ion conductivity, demonstrate superior oxidative stability, and be cost-effective.

Proton exchange membranes (PEMs) inherently possess negatively charged groups, typically sulfonic acid ($-SO_3H$) moieties, which ionize to release H^+ ions and facilitate the exchange of positive ions in the electrolyte. Currently, Nafion membranes, i.e., perfluorosulfonic acid membranes produced by Chemours, achieve voltage efficiencies exceeding 90% in VRFBs due to their remarkable proton conducting capability.[7,10,11] However, their widespread adoption is still

Received: December 9, 2024
Revised: February 22, 2025
Accepted: February 24, 2025

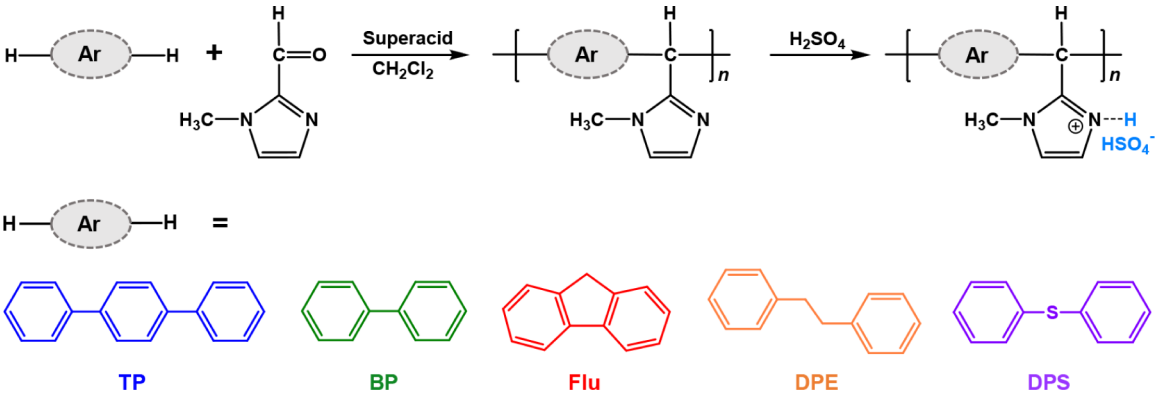

Figure 1. Synthesis of various poly(arylene methylimidazole) polymers.

hindered by high manufacturing costs and significant electrolyte cross-contamination due to vanadium ion permeation.[8,12,13] Instead, low-cost sulfonated aromatic polymer membranes incorporating sulfonic acid groups, such as sulfonated poly(ether sulfonate) (SPES)[14,15] and sulfonated poly(ether ether ketone) (SPEEK)[16,17,18] have been explored. Nevertheless, the negatively charged sulfonic acid groups increase the attraction to vanadium ions, promoting electrolyte migration.[6,8,19] Moreover, aryl ether bonds in the polymer backbone are susceptible to attack and degradation in environments with high vanadium ion concentrations, indicating a need for enhanced chemical stability in VRFB applications.[10,20]

In VRFBs, the electrolyte is sulfuric acid (SA), containing redox couples of varying valence states.[4,5] Consequently, several basic polymer membranes have been proposed for VRFB applications after doping with SA molecules to impart ion-conducting capabilities. A prominent example is polybenzimidazole (PBI), which features two benzimidazole groups per repeating unit. Zhou et al.[21] were the first to employ PBI membranes in VRFBs, achieving significantly improved Coulombic efficiencies of up to 99% within the current density range of 20 to 80 mA cm^{-2}. The SA-doped PBI membrane demonstrated low vanadium ion permeability because the protonated PBI chains repel positively charged vanadium ion species through electrostatic exclusion.[22] However, the high area resistance (AR) inherent in PBI-based VRFBs leads to reduced voltage and energy efficiencies.[21,23] To address this issue, various strategies have been employed to enhance the SA uptake of PBI membranes, thereby lowing AR, including the fabrication of porous membranes,[4,24] blending with polymers that have superior SA adsorption capacities,[25,26] grafting long side chains or basic groups[27,28] and employing preswelling techniques.[6,29,30−32]

In addition to PBI, other membranes containing basic groups have been developed by our group and others, including polyvinylpyrrolidone (PVP),[33−35] poly(ethylene imine) (PEI),[36] poly(arylene piperidine),[37−40] poly(arylene pyridine),[23,41,42] and poly(*p*-terphenylene methylimidazole).[43] Among these basic group containing polymers, membranes featuring π-conjugated *N*-heterocyclic structures exhibit outstanding chemical stability. For instance, aryl ether-free poly(*p*-terphenyl-*co*-acetylpyridine) (PTAP) was synthesized via a straightforward superelectrophilic activation polymerization using para-terphenyl and 4-acetylpyridine as reactants.[41] The PTAP polymer we synthesized displayed excellent solubility in organic solvents, and the corresponding membrane exhibited SA absorption capacity and excellent chemical stability. It also showed satisfactory permeability to vanadium ions, primarily due to electrostatic repulsion between the vanadium ions and protonated pyridine rings, resulting in excellent ion selectivity for the SA doped PTAP membrane. Furthermore, in our previous work, we synthesized poly(*p*-terphenylene methylimidazole) using the highly reactive monomer of 1-methyl-2-imidazolecarboxaldehyde.[43] The resulting imidazole-containing membrane displayed excellent chemical stability against high-valence vanadium ions and high sulfonic acid absorption capacity, resulting from the presence of pendant imidazole rings.

In this study, we build upon our previous work[43] by synthesizing a series of methylimidazole-containing polymers through a straightforward superacid-catalyzed polymerization of 1-methyl-2-imidazolecarboxaldehyde with five different aromatic monomers: biphenyl, fluorene, 1,2-diphenylethane, diphenyl sulfide, and *p*-terphenyl as a reference. This approach aims to investigate how variations in the chemical structure of the polymer backbone affect membrane properties for VRFB applications. Our design strategy employs basic imidazole groups to provide acidic sites for ion transport via hydrogen bonding, while modifications in the aromatic monomer structures adjust the polymer microstructure to optimize area resistance and ionic selectivity, achieving high-performance membranes for VRFB applications. We systematically examined the influence of different aromatic monomers on the polymer structure and their physicochemical properties, and further evaluated the electrochemical performance and cycling stability of the membranes in VRFB operations.

2. EXPERIMENTAL SECTION

2.1. Materials. *p*-Terphenyl (TP), biphenyl (BP), fluorene (Flu), 1,2-diphenylethane (DPE), diphenyl sulfide (DPS) and 1-methyl-2-imidazolecarboxaldehyde (MeIm) were procured from Adamas Reagent Ltd. Dichloromethane (DCM), trifluoromethanesulfonic acid (TFSA) and trifluoroacetic acid (TFA) were obtained from Energy Chemical Co., Ltd. Sulfuric acid (H_2SO_4) and magnesium sulfate ($MgSO_4$) were purchased from Sinopharm Chemical Reagent Co. Ltd. Vanadium(IV) sulfate oxide hydrate ($VOSO_4$) was sourced from Haizhongtian Chemical Company in Shenyang, China.

2.2. Synthesis of Poly(arylene methylimidazole) Membranes. All poly(arylene methylimidazole) polymers were synthesized using a modified superacid-catalyzed polymerization based on our previous study.[43] For example, the synthesis of poly(methylimidazole biphenyl) (P(MeIm-*co*-BP)) proceeded as follows. Biphenyl (1.37 g, 8.88 mmol) and 1-methyl-2-imidazolecarboxaldehyde (1.27 g, 11.55 mmol) were added into a 100 mL two-neck round-bottom flask with mechanical stirring and dissolved in 2 mL of

https://doi.org/10.1021/acsapm.4c03945
ACS Appl. Polym. Mater. XXXX, XXX, XXX−XXX

DCM. While maintaining the mixture in an ice bath, TFSA (6 mL) gradually added. Mechanical stirring reaction about 15 min, the solution had a high viscosity, poured it into 1 M $NaHCO_3$ solution. The resulting light yellow fibers were thoroughly washed with deionized water until the filtrate was neutral. The final polymer was obtained after drying in an oven at 80 °C. By replicating the BP monomer with TP, Flu, DPE or DPS, four additional poly(arylene methylimidazole) polymers were synthesized, named P(MeIm-*co*-TP), P(MeIm-*co*-Flu), P(MeIm-*co*-DPE) and P(MeIm-*co*-DPS), respectively. The synthesis procedure and chemical structures of these five poly(arylene methylimidazole) polymers are illustrated in Figure 1.

Membranes were fabricated through a solution casting method from 2.0 wt % polymer solutions. The solutions were magnetically stirred until clear and transparent, which were then filtered and poured onto Petri dishes. After dried in an oven at 80 °C for 12 h, the transparent membranes were peeled off, washed thoroughly, and dried again.

2.3. Characterizations. An internal standard of tetramethylsilane was utilized, with DMSO-d_6 serving as solvents for various polymers. Each polymer's proton nuclear magnetic resonance (^{1}H NMR) spectra were acquired using a Bruker AVANCE 400 MHz spectrometer. After platinum coating, the surface morphology of all membranes was examined using an SU-8010 scanning electron microscope. Membrane samples were cut into dumbbell shapes (25 mm in length and 4 mm in width), and tensile stress−strain curves were collected at a rate of 5 mm min^{-1} using a CMT2000 electronic tensile testing machine at room temperature.

The inherent viscosity (η) of the polymer was determined at 30 °C using an Ubbelohde viscometer. The polymer was dissolved in DMSO and diluted to a concentration (c) of 100 mg dL^{-1}. Each polymer solution was measured in triplicate. The calculation of the viscosity is based on the following eq 1

$$\eta = \ln\left(\frac{t_x}{t_0}\right)/c \tag{1}$$

Where t_x and t_0 refer to the flow times of the polymer/DMSO solution and the blank DMSO solution, respectively.

The well-known proton transfer advantages of SA doped membranes,[4,44] make acid uptake (AU%) a crucial parameter for evaluating their physicochemical properties. After drying, the initial dimensions (L_0, W_0, D_0) and mass (m_0) of the membranes were recorded. The membranes were then submersed in a 3 M H_2SO_4 solution at 30 °C. Periodically, samples were removed, gently blotted with filter paper, weigh its quality, and repeat the above operation many times until the quality of the membrane is balanced. The dimensions (L_1, W_1, D_1) and the mass (m_1) of the acid doped membrane were measured. AU% was calculated using eq 2, while the percentages of swelling in area (SA%) and volume (SV%) were determined using eqs 3 and 4, respectively.[44]

$$AU\% = \frac{m_1 - m_0}{m_0} \times 100\% \tag{2}$$

$$SA\% = \frac{L_1 \times W_1 - L_0 \times W_0}{L_0 \times W_0} \times 100\% \tag{3}$$

$$SV\% = \frac{L_1 \times W_1 \times D_1 - L_0 \times W_0 \times D_0}{L_0 \times W_0 \times D_0} \times 100\% \tag{4}$$

Electrochemical impedance spectroscopy (EIS) measurements for the SA doped membranes in 3 M H_2SO_4 were performed using an electrochemical workstation spanning frequencies from 100 MHz to 1 Hz.[4,23] An H-type electrolytic cell with an effective diffusion area of 2.27 cm^2 was used for testing. Surface resistance was determined using eq 5, where R_0 represents the resistance of the sulfuric acid without the membrane, and R_1 is the resistance of the test membrane.

$$AR = (R_1 - R_0) \times A \tag{5}$$

where A is the effective area (2.27 cm^2) between the two diffusion cells.

To evaluate VO^{2+} permeability, a diffusion cell with an effective area of 1.69 cm^2 was employed, containing 80 mL of 3 M H_2SO_4 solution with equal concentrations (1.5 M) of $VOSO_4$ and $MgSO_4$ to balance osmotic pressure.[12,21] The cell was magnetically stirred to minimize concentration polarization effects. The concentration of VO^{2+} ion in the $MgSO_4$ compartment was periodically measured using a PerkinElmer Lambda 750s UV−visible spectrometer. Permeability was then calculated according to eq 6.

$$P = \frac{LV_b}{A(C_a - C_b(t))}\frac{\mathrm{d}(C_b(t))}{\mathrm{d}t} \tag{6}$$

In this equation, V_b is the volume of the vanadium ion solution, C_a and $C_b(t)$ are the initial concentration of VO^{2+} and its concentration in the $MgSO_4$ solution at time t, respectively. A denotes the effective area, L is the membrane thickness, and P is the vanadium ion permeability coefficient.

Oxidation resistance was evaluated using a procedure similar to that described in previous reports.[22,29] The dried membrane was initially submersed in a 1.5 M VO_2^+/3 M H_2SO_4 solution for 12 h. After immersion, the membrane was carefully taken out, washed with deionized water, dried, and weighed again. For extended oxidation resistance testing, the membrane was periodically reimmersed in the same solution, and weight retention was determined by measuring any changes in mass.

2.4. VRFB Performance. The VRFB testing setup was as previously described in our earlier studies.[23,33] Graphite felt electrodes (9 cm^2) were utilized in our experiments. To evaluate the charge−discharge cycling performance, a Neware CT-4008 (5 V/12 A) battery testing system was used at current densities ranging from 160 mA cm^{-2} down to 40 mA cm^{-2}, and from 300 mA cm^{-2} down to 50 mA cm^{-2}. Long-term cycling stability was assessed at a constant current density of 100 mA cm^{-2}. To prevent electrode corrosion and hydrogen evolution during testing, the cell voltage was maintained between 1.65 and 1 V.[33] Coulombic efficiency (CE), energy efficiency (EE), and voltage efficiency (VE) were calculated according to eqs 7, 8, and 9, respectively.[4]

$$CE = \frac{\int I_d\,\mathrm{d}t}{\int I_c\,\mathrm{d}t} \times 100\% \tag{7}$$

$$EE = \frac{\int V_d I_d\,\mathrm{d}t}{\int V_c I_c\,\mathrm{d}t} \times 100\% \tag{8}$$

$$VE = \frac{EE}{CE} \times 100\% \tag{9}$$

Where d and c represent the discharge and charging process, and I, V, and t represent current, voltage, and time, respectively.

3. RESULTS AND DISCUSSION

3.1. Synthesis of Polymers and Fabrication of P(MeIm-*co*-X) Membranes. The polymer chemistry significantly influences the microstructure and performance of membranes.[45] Previous research has shown that biphenyl has a central torsion angle of about 45° at equilibrium, which is limited rotatable,[46] while the fluorene structure has a dihedral angle close to 0° demonstrating its high rigidity.[47] 1,2-Diphenyl ethane and diphenyl sulfide are flexible monomers, which are freely rotatable due to the existence of the ethylidene chain or thioether bond between benzene rings. In this study, by adjusting the chemical structures of aromatic monomers, five different poly(arylene methylimidazole) polymers including P(MeIm-*co*-TP), P(MeIm-*co*-BP), P(MeIm-*co*-Flu), P-(MeIm-*co*-DPE) and P(MeIm-*co*-DPS), were successfully synthesized using the straightforward Friedel−Crafts polymer-

https://doi.org/10.1021/acsapm.4c03945
ACS Appl. Polym. Mater. XXXX, XXX, XXX−XXX

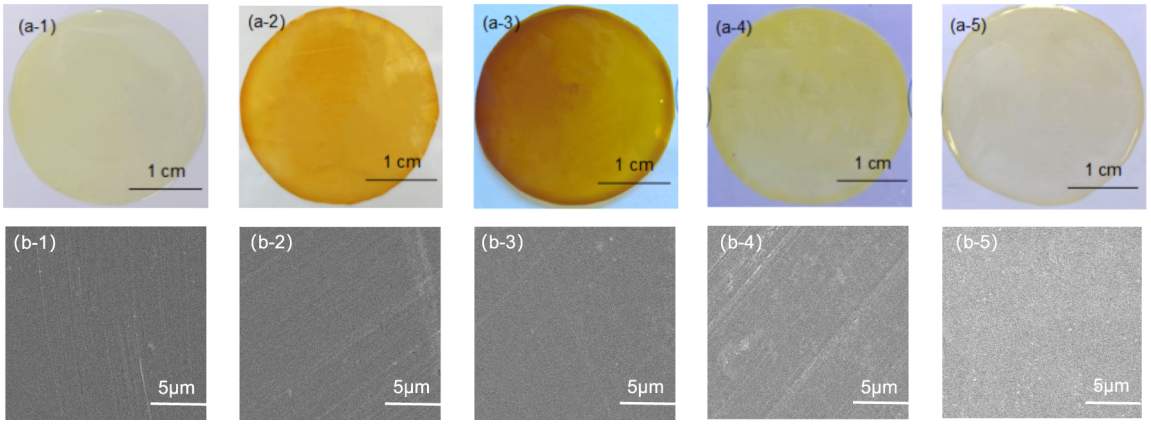

Figure 2. (a) Photographic and (b) SEM images of (1) P(MeIm-*co*-TP), (2) P(MeIm-*co*-BP), (3) P(MeIm-*co*-Flu), (4) P(MeIm-*co*-DPE), and (5) P(MeIm-*co*-DPS) membranes.

ization. Owing to the high reactivity of the MeIm monomer, these polymers exhibited elevated η values of 0.902, 0.767, 1.677, 2.304, and 2.768 dL g^{-1}, respectively.

All the synthesized polymers exhibited excellent solubilities in organic solvents including DMAc, DMF, DMSO and NMP at room temperature under magnetic agitation. This enhanced solubility can possibly result from the presence of tetrahedral sp^3 carbon atoms in the polymer backbone. Due to their excellent solubility, the sample solution casting method was used to prepare membranes. As shown in Figure 2, all poly(arylene methylimidazole) membranes exhibited a uniformly transparent appearance with a light-yellow coloration. Furthermore, the SEM images reveal that these membranes possess a dense and nonporous microstructure.

3.2. Chemical Structures of P(MeIm-*co*-X) Polymers.

The chemical structures of a series of P(MeIm-*co*-*X*) polymers were analyzed using ^{1}H NMR spectroscopy. As shown in Figure 3, all polymers exhibit signal peaks between 7.0 and 8.0 ppm, corresponding to the aromatic protons in the main chain. Taking P(MeIm-*co*-Flu) as an example, the characteristic proton bands at 3.51 and 5.82 ppm result from the methyl group (H_d) and the C−H bond (H_a) of methylimidazole, respectively.[43] The hydrogen peaks of the methylimidazole ring appear at 7.11 ppm (H_c) and 6.90 ppm (H_b). Moreover, a prominent characteristic peak is observed at 3.78 ppm (H_3), attributed to the $-CH_2-$ group in the fluorene moieties of the main chain.[48] Additionally, in the spectrum of P(MeIm-*co*-DPE), the characteristic peak assigned to the methylene linkage between two phenyl groups is observed at 2.86 ppm (H_3).[42] Characteristic peaks of the other polymers were assigned in the ^{1}H NMR spectra accordingly. Thus, these ^{1}H NMR results prove the successful synthesis of the series of P(MeIm-*co*-*X*) polymers.

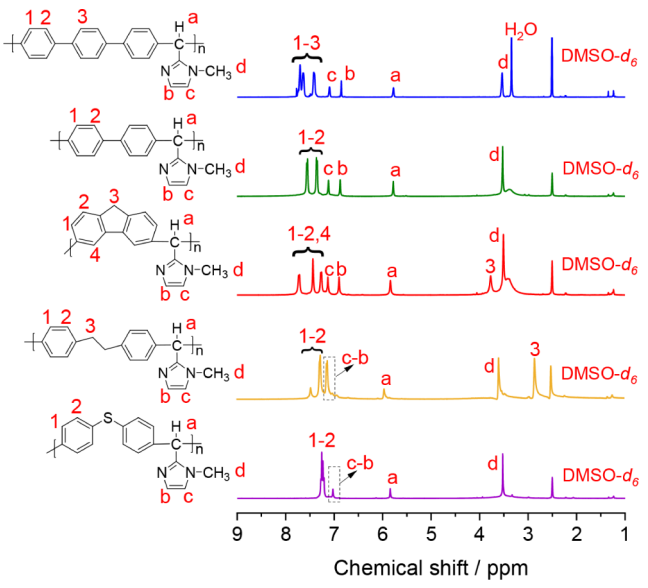

Figure 3. ^{1}H NMR spectra of P(MeIm-*co*-TP), P(MeIm-*co*-BP), P(MeIm-*co*-Flu), P(MeIm-*co*-DPE), and P(MeIm-*co*-DPS) polymers.

3.3. SA Uptake, Swelling, and Mechanical Properties.

Figure 4a shows the acid uptake (AU), area swelling (AS), and volume swelling (VS) of various membranes after immersion in a 3.0 mol L^{-1} H_2SO_4 solution at room temperature. Generally, both area swelling and volume swelling of the membranes increased with higher acid uptake. For example, the P(MeIm-*co*-BP) membrane had the highest AU value of 90%, correspondingly exhibiting the highest VS% of 68.9%. When the biphenyl units were replaced by terphenyl units, the P(MeIm-*co*-TP) membrane displayed a lower AU% of 59%, mainly due to the increased hydrophobicity of the P(MeIm-*co*-TP) polymer chains. When the biphenyl units were replaced by flexible ethylene linkages or thioether bonds, the AU% values of P (MeIm-*co*-DPE) and P (MeIm-*co*-DPS) are 54% and 64%, respectively. Interestingly, the P(MeIm-*co*-Flu) membrane had the second highest AU of 79% but exhibited the lowest AS and VS among the five membranes, at 4.9% and 20.9%, respectively. The addition of fluorene units could decrease rotational flexibility, which hindered polymer chain packing and enhanced intrachain rigidity, resulting in increased internal free volume.[49,50] Thus, the P(MeIm-*co*-Flu) membrane exhibited a high SA uptake without causing excessive swelling, thereby maintaining the mechanical properties of the membrane and preventing the penetration of vanadium ions.

The effective use of membranes in VRFBs critically depends on their mechanical properties. Membranes must possess adequate mechanical strength to endure external stresses arising from operational conditions like stack assembly and electrolyte circulation.[38] Figure 4b and Table S1 depict the mechanical properties of various membranes. The SA doped P(MeIm-*co*-TP) membrane exhibited the highest tensile strength of 44.6 MPa due to its rigid polymer skeleton. In contrast, the P(MeIm-*co*-DPE) membrane possessed the

https://doi.org/10.1021/acsapm.4c03945
ACS Appl. Polym. Mater. XXXX, XXX, XXX−XXX

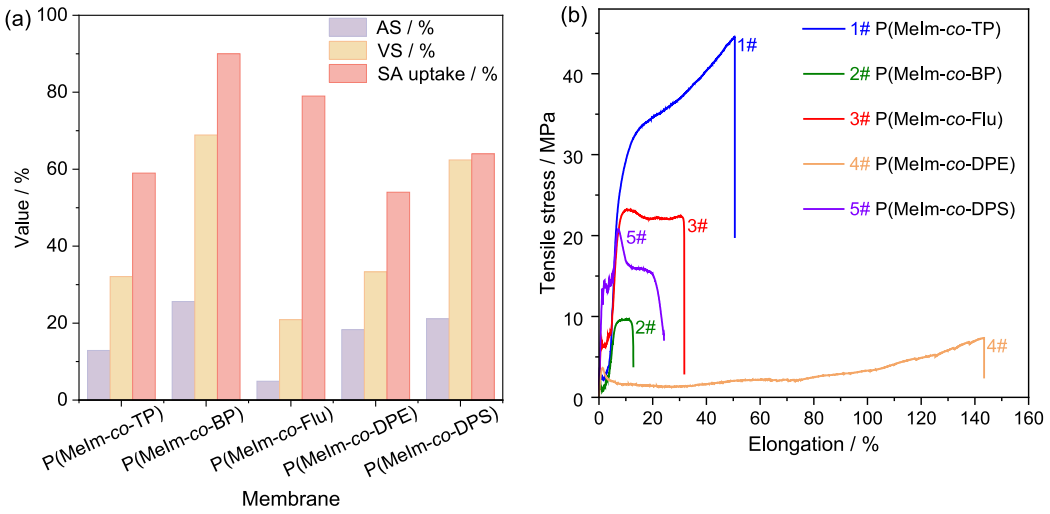

Figure 4. (a) SA uptake, dimensional swellings and (b) tensile stress−strain curves of various membranes after immersion in 3 mol L^{-1} SA solution at RT.

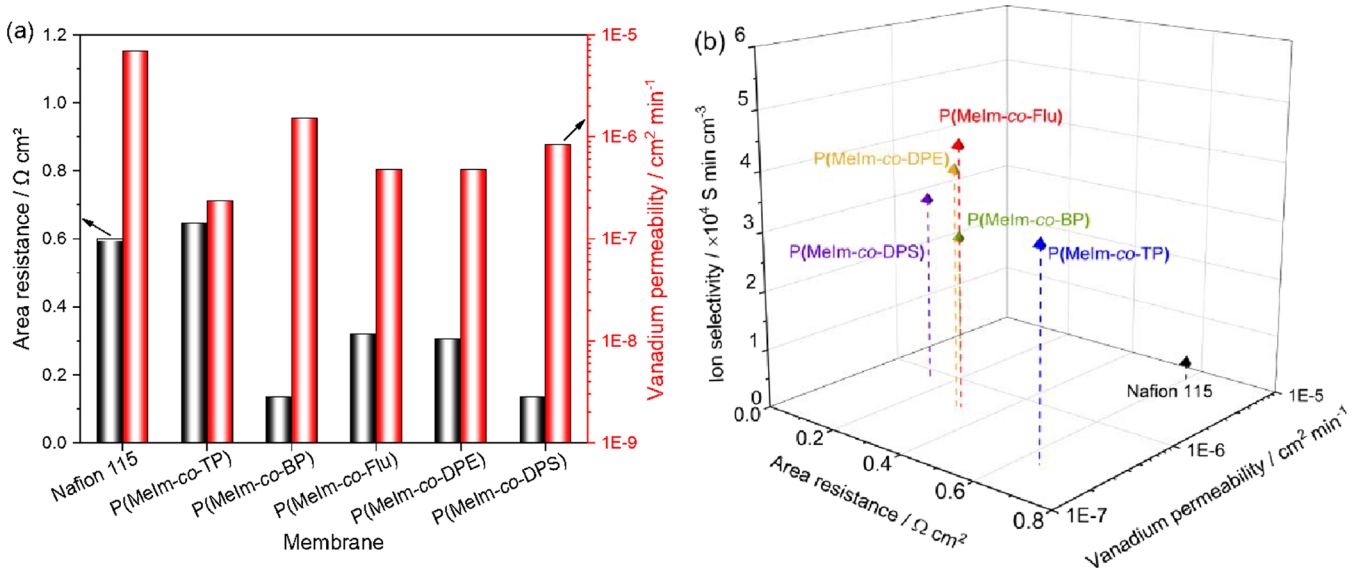

Figure 5. (a) AR and vanadium ion permeability and (b) ion selectivity of various SA-doped membranes.

lowest mechanical strength of 7.3 MPa and the largest elongation of 143%, owing to the presence of flexible polymer chains. As for P(MeIm-*co*-BP), its tensile strength was as low as 9.6 MPa due to its high acid uptake and swelling. Additionally, the viscosity of P(MeIm-*co*-Flu) is 1.677 dL g^{-1}, which is lower than that of P(MeIm-*co*-DPE) and P(MeIm-*co*-DPS). However, the P(MeIm-*co*-Flu) membrane demonstrated a relatively high tensile strength of 22.4 MPa, despite having a high AU% of 79%. This excellent mechanical performance of the P(MeIm-*co*-Flu) membrane could be attributed to its low volume swelling and the rigid planar structure of fluorene.

3.4. Area Resistance, Vanadium Ion Permeability and Ion Selectivity. For VRFBs, the membrane is required to possess a relatively low AR, as the AR significantly impacts both voltage and energy efficiencies.[4,28] Figure 5a shows the AR of various SA doped P(MeIm-*co*-*X*) membranes, with Nafion 115 included as a reference. In this work, all the SA doped P(MeIm-*co*-*X*) membranes had a thickness of approximately 50 μm as listed in Table S2. Compared to the AR of Nafion 115 (0.60 Ω cm^2), the P(MeIm-*co*-TP) membrane exhibited a slightly higher AR of 0.65 Ω cm^2, while the other membranes showed lower ARs. Notably, the P(MeIm-*co*-BP) membrane, having the highest SA absorption, possessed the lowest AR of 0.13 Ω cm^2 (Figure 5a) and the highest conductivity of 35.2 mS cm^{-1} (Table S2), indicating a high ion migration rate. However, this might result in serious vanadium ion crossover. As for the P(MeIm-*co*-DPE) and P(MeIm-*co*-DPS) membranes with flexible linkages, their ARs were 0.31 Ω cm^2 and 0.14 Ω cm^2, respectively. The P(MeIm-*co*-Flu) membrane had a suitable AR of 0.32 Ω cm^2. The low ARs of the SA doped P(MeIm-*co*-*X*) membranes were attributed to the presence of freely rotating pendant methylimidazole groups, which were protonated by SA molecules and formed effective ionic conduction channels. Meanwhile, the AR results indicate that the aromatic structure of P(MeIm-*co*-*X*) has a great influence on the ionic conduction capabilities of the membranes.

High vanadium ion permeability can result in severe self-discharge and a decline in CE, which is a significant factor

https://doi.org/10.1021/acsapm.4c03945
ACS Appl. Polym. Mater. XXXX, XXX, XXX−XXX

influencing the application of membranes in VRFBs.[28,51] Figure 5a presents the vanadium ion permeability of various SA doped P(MeIm-*co*-*X*) membranes. As shown, the Nafion 115 membrane demonstrated the largest vanadium ion permeability of 6.94×10^{-6} cm^2 min^{-1}. Owing to the excessive swelling, the P(MeIm-*co*-BP) membrane exhibited a relatively high vanadium ion permeability, reaching 1.52×10^{-6} cm^2 min^{-1}. For the other membranes, the vanadium ion permeability values were 2.36×10^{-7} cm^2 min^{-1}, 4.80×10^{-7} cm^2 min^{-1}, 4.80×10^{-7} cm^2 min^{-1}, and 8.35×10^{-7} cm^2 min^{-1} for the P(MeIm-*co*-TP), P(MeIm-*co*-Flu), P(MeIm-*co*-DPE), and P(MeIm-*co*-DPS), respectively. These values are approximately 1 order of magnitude lower than that of the Nafion 115 membrane. The excellent vanadium ion resistance of above-mentioned P(MeIm-*co*-*X*) membranes result from the Donnan effect of the protonated methylimidazole groups in the polymers, which exerted a repulsive force on vanadium ions.[52]

The ion selectivity of membranes exhibits a considerable impact on the performance of VRFBs.[11] In order to comprehensively incorporate the impacts of AR and vanadium ion permeability, the ion selectivity of all membranes was calculated accordingly. As depicted in Figure 5b, the P(MeIm-*co*-Flu) membrane demonstrated the highest ion selectivity, reaching up to 4.43×10^4 S min cm^{-3}, which is because of its relatively low AR and permeability of vanadium ions. The outstanding ion selectivity indicates that protons migrated more easily than vanadium ions within the P(MeIm-*co*-Flu) membrane.[38,53] Additionally, the P(MeIm-*co*-TP) (3.48×10^4 S min cm^{-3}), P(MeIm-*co*-BP) (2.32×10^4 S min cm^{-3}), P(MeIm-*co*-DPE) (4.01×10^4 S min cm^{-3}), and P(MeIm-*co*-DPS) (3.16×10^4 S min cm^{-3}) membranes all exhibited much higher ion selectivity than Nafion 115 (0.31×10^4 S min cm^{-3}). These findings indicate that incorporating methylimidazole groups into P(MeIm-*co*-*X*) membranes enhances the balance between ion conduction and vanadium ion permeability.

3.5. Chemical Stability. The chemical stability of polymer membranes signifies their capacity to resist the harsh chemical environments encountered in VRFBs. Membrane degradation due to attack by highly oxidative VO_2^+ ions in the electrolyte leads to poor stability of the membranes.[20] In this study, different membranes were submersed in a 1.5 M VO_2^+ and 3.0 M H_2SO_4 solution at room temperature to assess the chemical stability of membranes. As depicted in Figure 6, the mass retention percentage of different P(MeIm-*co*-*X*) membranes during the chemical stability measurement and includes morphological photographs of the membranes before and after 400 h. Owing to the adsorption of SA molecules and vanadium ions, all the P(MeIm-*co*-*X*) membranes exhibited an initial increase in mass during the first 12 h, which was also indicated by a color change in the membranes.[43,44] As seen from Figure 6, after 400 h of oxidative testing, the P(MeIm-*co*-TP), P(MeIm-*co*-BP), and P(MeIm-*co*-Flu) membranes all maintained their initial shape without fragmentation and kept their mass stable. However, the P(MeIm-*co*-DPE) and P(MeIm-*co*-DPS) membranes with flexible linkages were broken and retained only 32.7% and 88.9% of their initial mass after 400 h, respectively. In contrast, the P(MeIm-*co*-Flu) membrane with intrinsic rigid chain structure maintained its intact shape and stable mass after the 400-h chemical stability test, probably due to its low swelling. Consequently, the P(MeIm-*co*-TP), P(MeIm-*co*-BP) and P(MeIm-*co*-Flu) membranes exhibited good stability under strongly acidic and highly oxidative conditions, making them more advantageous as separators for VRFB applications.

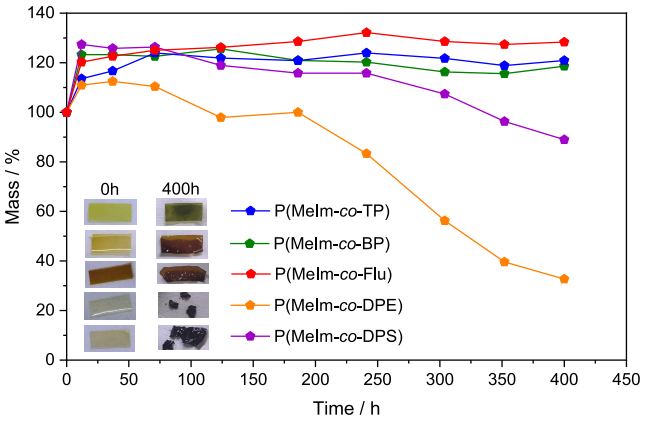

Figure 6. Mass retention of various membranes in 1.5 M VO_2^+ and 3 M SA solution at room temperature, and photos of corresponding membranes before (0 h) and after (400 h) test.

3.6. VRFB Performance. Figure 7a shows the charge−discharge curves at 100 mA cm^{-2} of VRFBs based on various P(MeIm-*co*-*X*) and Nafion 115 membranes. Membranes with higher AR generally have higher charging voltages and lower discharging voltages, resulting in shorter charging time.[43,53] It can be observed from the figure that, except for the P(MeIm-*co*-TP) membrane, all other P(MeIm-*co*-*X*) membranes had lower charging voltages and higher discharging voltages compared to Nafion 115. As depicted in Figure 5a, the P(MeIm-*co*-TP) membrane exhibited a higher AR than Nafion 115, while the other P(MeIm-*co*-*X*) membranes had lower ARs. Figure 7b presents the CE and VE of VRFBs based on P(MeIm-*co*-*X*) and Nafion 115 membranes. From the figure, it can be observed that CEs of the P(MeIm-*co*-BP), P(MeIm-*co*-DPE) and P(MeIm-*co*-DPS) membranes gradually decreased with extended battery operation time, especially under low current densities of 40−80 mA cm^{-2}. This decline is likely because of their high vanadium ion permeability or poor chemical stability. In contrast, as the current density increased, the CEs of the P(MeIm-*co*-TP), P(MeIm-*co*-Flu) and Nafion 115 membranes slightly improved. This is because that the charge−discharge time became shorter with increased current density, which reduced the number of vanadium ions which could cross over during one cycle.[28,54] Furthermore, the CEs of the P(MeIm-*co*-TP) and P(MeIm-*co*-Flu) membranes were larger than CE of Nafion 115, attributed to the better vanadium ion resistance of those membranes. At the same time, the VE of the aforementioned three membranes increased with decreasing current density, due to more pronounced ohmic polarization and overpotential at higher current densities.[43,55] At a certain current density, the VE corresponded to the AR. For instance, the VRFB based on the P(MeIm-*co*-Flu) membrane exhibited a higher VE of 86.1% at 100 mA cm^{-2} compared to P(MeIm-*co*-TP) and Nafion 115, which had VEs of 76.0% and 78.2%, respectively. This is clearly due to its lower AR. Figure 7c shows the EE results of various batteries at different current densities. For the P(MeIm-*co*-TP) membrane, it displayed lower EEs than Nafion 115 at 100−160 mA cm^{-2} but higher EEs at 40−80 mA cm^{-2}, obviously because of the higher AR and lower vanadium ion permeability compared to Nafion 115. Due to its high ion selectivity, the

https://doi.org/10.1021/acsapm.4c03945
ACS Appl. Polym. Mater. XXXX, XXX, XXX−XXX

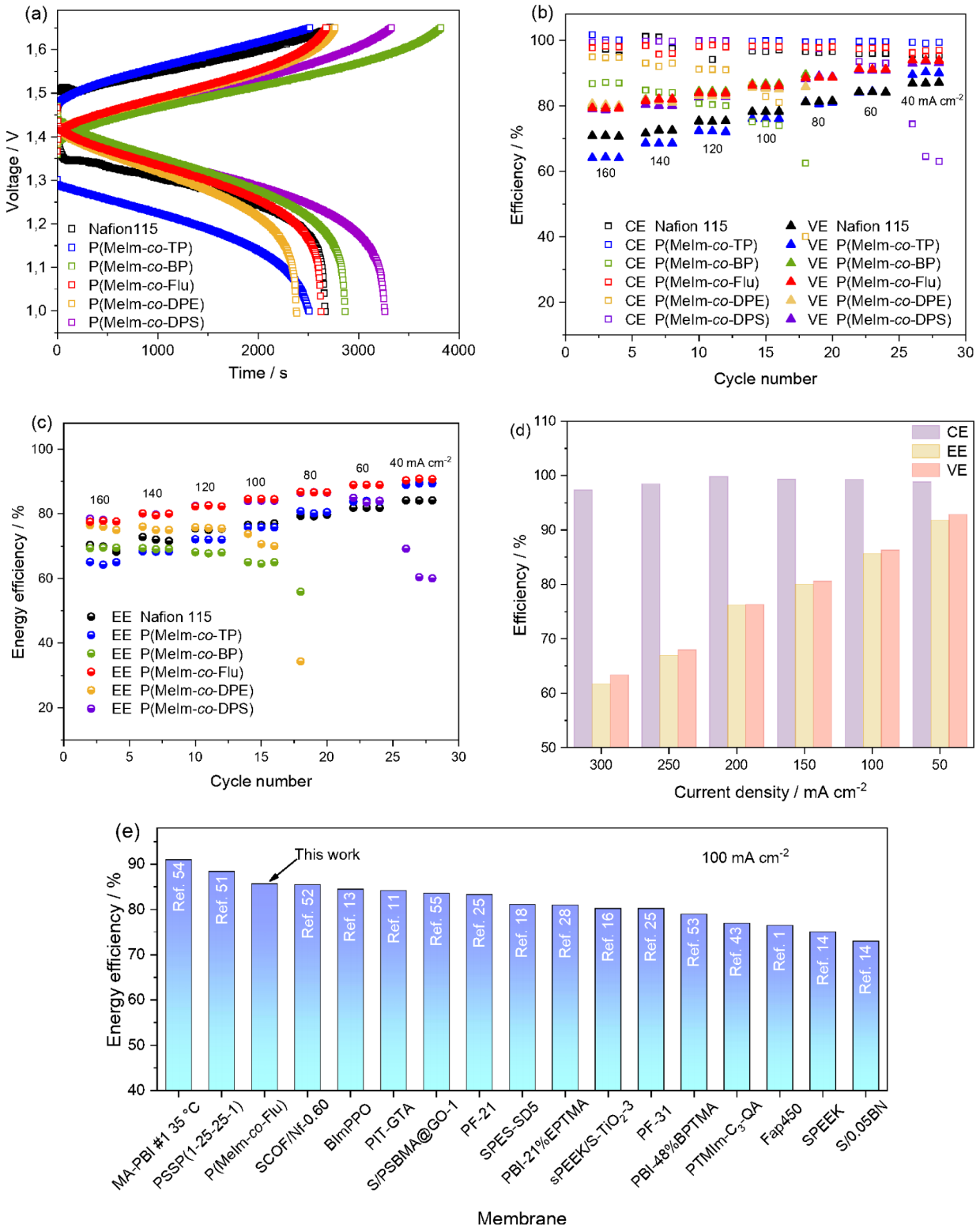

Figure 7. (a) Charge−discharge curves at 100 mA cm^{-2}; (b) CE and VE; and (c) EE of VRFBs assembled with Nafion 115 and various P(MeIm-*co*-*X*) membranes at 40−160 mA cm^{-2}; (d) CE, VE, and EE of the VRFB based on P(MeIm-*co*-Flu) at 50−300 mA cm^{-2}; (e) comparison of EE of VRFBs using various membranes from this work and the literature at 100 mA cm^{-2}.

VRFB based on the P(MeIm-*co*-Flu) membrane achieved the highest EEs at all current densities. For instance, at 100 mA cm^{-2}, the EE of the P(MeIm-*co*-Flu) membrane was 85.7%, exceeding the EEs of the P(MeIm-*co*-TP) and Nafion 115 membranes, which were 75.8% and 76.5%, respectively.

Operating VRFBs at higher current densities can increase the output power density, reduce stack size, and lower manufacturing costs.[11] Therefore, the performance of the VRFB based on the P(MeIm-*co*-Flu) membrane was further evaluated ranging from 50 mA cm^{-2} to 300 mA cm^{-2}, as depicted in Figure 7d. The results show that the battery

https://doi.org/10.1021/acsapm.4c03945
ACS Appl. Polym. Mater. XXXX, XXX, XXX−XXX

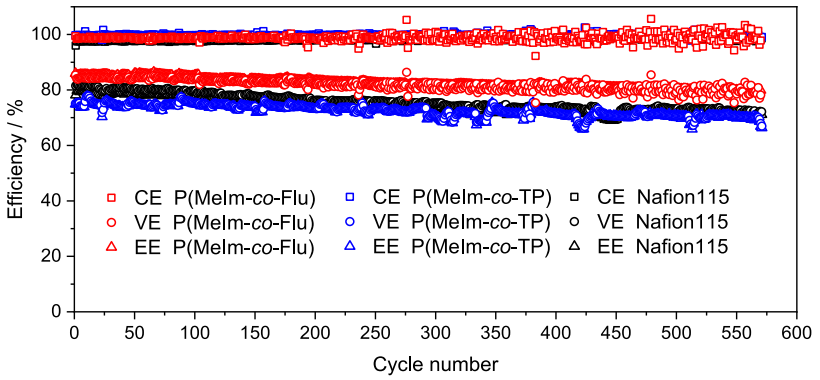

Figure 8. CE, VE, and EE of VRFBs with P(MeIm-*co*-TP), P(MeIm-*co*-Flu), and Nafion 115 membranes at 100 mA cm^{-2}.

performance based on the P(MeIm-*co*-Flu) membrane was excellent. At a high current density of 300 mA cm^{-2}, the P(MeIm-*co*-Flu) based VRFB still exhibited high CE, VE and EE of 97.3%, 63.4% and 61.7%, respectively. Additionally, compared to most other membranes previously reported for VRFBs, the P(MeIm-*co*-Flu) membrane still possessed a superior EE value at 100 mA cm^{-2}, as shown in Figure 7e. Henkensmeier et al. prepared sulfonated para-PBI membranes, which achieved much better EE values, such as 91% at 100 mA cm^{-2}.[54] It also should be noted that similar EE values may be achieved for P(MeIm-*co*-Flu) membrane with lower thickness, but it is clear that thicker membrane is more suitable for stable operation. In summary, due to its simultaneously low vanadium ion permeability and low AR, the battery based on the P(MeIm-*co*-Flu) membrane demonstrated superior battery efficiency performance.

As depicted in Figures 8 and S1, we evaluated the long-term VRFB cycling stability of P(MeIm-*co*-Flu), P(MeIm-*co*-TP), and Nafion 115 membranes without balancing the electrolyte during the VRFB operation, based on the VRFB performance as discussed above. It should be noted that the efficiencies of the P(MeIm-*co*-BP), P(MeIm-*co*-DPE) and P(MeIm-*co*-DPS) membranes significantly decreased within 50 cycles during battery operation, mainly because of the high vanadium ion permeability or poor chemical stability. In contrast, the VRFBs with P(MeIm-*co*-Flu) and P(MeIm-*co*-TP) membranes demonstrated excellent cycling stability, with their CE, VE and EE remaining relatively stable over 570 cycles. Meanwhile, the CE of the battery equipped with Nafion 115 was around 98%, while its EE decreased from 79.5% to 70.8%. For the P(MeIm-*co*-Flu) membrane, its CE remained around 99.0%, while EE decreased from 85.4% to 80.9%, indicating higher cycling efficiency and a lower VRFB decay rate. Therefore, the P(MeIm-*co*-Flu) membrane, with its outstanding VRFB performance and cycling stability, can be considered a promising candidate for VRFBs and other electrochemical energy devices.

4. CONCLUSIONS

Five ether-free poly(arylene methylimidazole) copolymers were synthesized through an efficient superacid-catalyzed polymerization of 1-methyl-2-imidazolecarboxaldehyde with five distinct aromatic monomers: biphenyl, fluorene, 1,2-diphenylethane, diphenyl sulfide, and *p*-terphenyl. Incorporating basic methylimidazole groups enhanced SA absorption and facilitated ion transport via hydrogen bonding. Our investigations demonstrated that the chemical structure of the aromatic units significantly influenced the membrane properties. Specifically, P(MeIm-*co*-DPE) and P(MeIm-*co*-DPS) membranes, containing flexible ethylidene chains and thioether bonds, exhibited high acid uptake but experienced excessive swelling and poor chemical stability. In contrast, the P(MeIm-*co*-TP) membrane with a rigid and hydrophobic terphenyl group showed low vanadium ion permeability, excellent mechanical strength, but high AR. Among all the membranes studied, P(MeIm-*co*-Flu) incorporating fluorene units exhibited the best overall performance, combining high tensile strength (22.4 MPa), low AR (0.32 Ω cm^2), low vanadium ion permeability (4.80×10^{-7} cm^2 min^{-1}), high ion selectivity (4.43×10^4 S min cm^{-3}), and outstanding chemical stability. Consequently, VRFB employing the P(MeIm-*co*-Flu) membrane achieved an EE of 85.7% at 100 mA cm^{-2}, surpassing that of Nafion 115 (76.5%) under the same conditions. Furthermore, over 570 cycles at 100 mA cm^{-2}, this membrane demonstrated excellent capacity retention, consistently maintaining CEs above 99% while EEs decreased slightly from 85.4% to 80.9%. In summary, we have developed a high-performance, easily synthesized, and cost-effective P(MeIm-*co*-Flu) membrane that showed significant potential for application in VRFBs.

■ ASSOCIATED CONTENT

Supporting Information

The Supporting Information is available free of charge at https://pubs.acs.org/doi/10.1021/acsapm.4c03945.

Mechanical properties, thickness and conductivity of various membranes after doping with 3 M SA; discharge capacity retention of VRFBs with Nafion 115, P(MeIm-*co*-TP) and P(MeIm-*co*-Flu) membranes at 100 mA cm^{-2} (PDF)

■ AUTHOR INFORMATION

Corresponding Authors

Jin Wang − *College of Pharmacy, Shenyang Medical College, Shenyang 110034, PR China*; Email: wangjin@symc.edu.cn

Jingshuai Yang − *Department of Chemistry, College of Sciences, Northeastern University, Shenyang 110004, China*; orcid.org/0000-0002-0275-0978; Email: yjs@mail.neu.edu.cn

Authors

Meichen Zhang − *Department of Chemistry, College of Sciences, Northeastern University, Shenyang 110004, China*

https://doi.org/10.1021/acsapm.4c03945
ACS Appl. Polym. Mater. XXXX, XXX, XXX−XXX

Peiru Lv − *Department of Chemistry, College of Sciences, Northeastern University, Shenyang 110004, China*
Lele Wang − *Department of Chemistry, College of Sciences, Northeastern University, Shenyang 110004, China*

Complete contact information is available at: https://pubs.acs.org/10.1021/acsapm.4c03945

Author Contributions

[§]M.Z. and P.L. contributed equally to this work. The manuscript was written through contributions of all authors.

Funding

We gratefully acknowledge the Liaoning Provincial Natural Science Foundation of China (2020-MS-087), the Science and Technology Major Project of Liaoning Province (Grant No. 2024JH1/11700015), and the Natural Science Foundation of China (52403273).

Notes

The authors declare no competing financial interest.

■ ACKNOWLEDGMENTS

We would like to express our gratitude to Prof. Jianguo Liu from the Institute of Metal Research, Chinese Academy of Sciences, for his assistance with the VRFB testing and discussions.

■ REFERENCES

(1) Thiam, B. G.; Ansary, Y. E.; Marbouh, M.; Magri, A. E.; Vaudreuil, S. A low-cost design approach to vanadium redox flow test cell. *Electrochim. Acta* **2024**, *494*, 144481.
(2) Zhou, X. J.; Xue, R.; Zhong, Y. G.; Zhang, Y.; Jiang, F. J. Asymmetric porous membranes with ultra-high ion selectivity for vanadium redox flow batteries. *J. Membr. Sci.* **2020**, *595*, 117614.
(3) Briot, L.; Petit, M.; Cacciuttolo, Q.; Pera, M. C. Aging phenomena and their modelling in aqueous organic redox flow batteries: a review. *J. Power Sources* **2022**, *536*, 231427.
(4) Che, X. F.; Zhao, H.; Ren, X. R.; Zhang, D. H.; Wei, H.; Liu, J. G.; Zhang, X.; Yang, J. S. Porous polybenzimidazole membranes with high ion selectivity for the vanadium redox flow battery. *J. Membr. Sci.* **2020**, *611*, 118359.
(5) Shi, Y.; Eze, C.; Xiong, B.; He, W.; Zhang, H.; Lime, T. M.; Ukilf, A.; Zhao, J. Recent development of membrane for vanadium redox flow battery applications: A review. *Appl. Energy* **2019**, *238*, 202−224.
(6) Dai, Q.; Xing, F.; Liu, X. N.; Shi, D. Q.; Deng, C. Z.; Zhao, Z. M.; Li, X. F. High-performance PBI membranes for flow batteries: from the transport mechanism to the pilot plant. *Energy Environ. Sci.* **2022**, *15*, 1594−1600.
(7) Chinese Society of Electrochemistry. Chinese Society of Electrochemistry, The Top Ten Scientific Questions in Electrochemistry. *J. Electrochem.* **2024**, *30* (1), 2024121.
(8) Thiamz, B. G.; Vaudreuil, S. Review—Recent Membranes for Vanadium Redox Flow Batteries. *J. Electrochem. Soc.* **2021**, *168* (7), 070553.
(9) Khataee, A.; Pan, D.; Olsson, J.; Jannasch, P.; Lindstrom, R. Asymmetric cycling of vanadium redox flow batteries with a poly(arylene piperidinium)-based anion exchange membrane. *J. Power Sources* **2021**, *483*, 229202−229207.
(10) Li, X. F.; Zhang, H. M.; Mai, Z. S.; Zhang, H. Z.; Vankelecom, I. Ion exchange membranes for vanadium redox flow battery (VRFB) applications. *Energy Environ. Sci.* **2011**, *4*, 1147−1160.
(11) Yang, J. S.; Lv, P. R.; Tang, W. Q.; Wang, Q. Sulfonate and Ammonium-Grafted Poly (isatin triphenyl) Membranes for the Vanadium Redox Flow Battery. *ACS Appl. Polym. Mater.* **2024**, *6*, 10727−10737.
(12) Düerkop, D.; Widdecke, H.; Schilde, C.; Kunz, U.; Schmiemann, A. Polymer membranes for all-vanadium redox flow batteries: a review. *Membranes* **2021**, *11*, 214.
(13) Li, J.; Xu, F.; Chen, W. S.; Han, Y. Y.; Lin, B. C. Anion Exchange Membranes Based on Bis-Imidazolium and Imidazolium-Functionalized Poly (phenylene oxide) for Vanadium Redox Flow Battery Applications. *ACS Omega* **2023**, *8*, 16506−16512.
(14) Fu, Z. M.; Liu, J. Y.; Liu, Q. F. SPEEK/PVDF/PES composite as alternative proton exchange membrane for vanadium redox flow batteries. *J. Electron. Mater.* **2016**, *45*, 666−671.
(15) Guo, D.; Zhou, X.; Zhang, Z.; Wang, F.; Jiang, F. Robust Ion-Selective Membrane for Redox Flow Batteries Based on Ultralow Sulfonation Degree Poly (Ether Sulfone). *Macromol. Chem. Phys.* **2021**, *222* (10), 2100015.
(16) Myures, X. M.; Suresh, S.; Arthanareeswaran, G. Construction of thermal, chemical and mechanically stable ion exchange membranes with improved ion selectivity for vanadium redox flow batteries applications. *J. Power Sources* **2024**, *591*, 233818.
(17) Sousa, J. F. M.; Pina, J.; Gomes, C.; Dias, L. D.; Pereira, M. M.; Murtinho, D.; Dias, P.; Azevedo, J.; Mendes, A.; de Melo, J. S. S.; Pais, A. A. C. C.; Pineiro, M.; Valente, A. J. M. Transport and photophysical studies on porphyrin-containing sulfonated poly (ether ether ketone) composite membranes. *Mater. Today Commun.* **2021**, *29*, 102781.
(18) Palanisamy, G.; Oh, T. H. TiO_2 containing hybrid composite polymer membranes for vanadium redox flow batteries. *Polymers* **2022**, *14*, 1617.
(19) Shin, D. W.; Guiver, M. D.; Lee, Y. M. Hydrocarbon-based polymer electrolyte membranes: importance of morphology on ion transport and membrane stability. *Chem. Rev.* **2017**, *117*, 4759−4805.
(20) Chen, D. Y.; Hickner, M. A. V^{5+} degradation of sulfonated radel membranes for vanadium redox flow batteries. *Phys. Chem. Chem. Phys.* **2013**, *15*, 11299−11305.
(21) Zhou, X. L.; Zhao, T. S.; An, L.; Wei, L.; Zhang, C. The use of polybenzimidazole membranes in vanadium redox flow batteries leading to increased coulombic efficiency and cycling performance. *Electrochim. Acta* **2015**, *153*, 492−498.
(22) Dong, Z. W.; Di, M. T.; Hu, L.; Gao, L.; Yan, X. M.; Ruan, X. H.; Wu, X. M.; He, G. H. Hydrophilic/hydrophobic-bi-comb-shaped amphoteric membrane for vanadium redox flow battery. *J. Membr. Sci.* **2020**, *608*, 118179.
(23) Mu, T.; Tang, W. Q.; Jin, Y. P.; Che, X. F.; Liu, J. G.; Yang, J. S. Ether-free poly(p-terphenyl-co-acetylpyridine) membranes with different thicknesses for vanadium redox flow batteries. *ACS Appl. Energy Mater.* **2022**, *5*, 11713−11722.
(24) Luo, T.; David, O.; Gendel, Y.; Wessling, M. Porous poly(benzimidazole) membrane for all vanadium redox flow battery. *J. Power Sources* **2016**, *312*, 45−54.
(25) Jung, M.; Lee, W.; Noh, C.; Konovalova, A.; Yi, G. S.; Kim, S.; Kwon, Y.; Henkensmeier, D. Blending polybenzimidazole with an anion exchange polymer increases the efficiency of vanadium redox flow batteries. *J. Membr. Sci.* **2019**, *580*, 110−116.
(26) Chen, F. Y.; Che, X. F.; Ren, X. R.; Zhao, L. N.; Zhang, D. H.; Chen, H.; Liu, J. G.; Yang, J. S. Polybenzimidazole and polyvinylpyrrolidone blend membranes for vanadium flow battery. *J. Electrochem. Soc.* **2020**, *167*, 060511.
(27) Jang, J. K.; Kim, T. H.; Yoon, S. J.; Lee, J. Y.; Lee, J. C.; Hong, Y. T. Highly proton conductive, dense polybenzimidazole membranes with low permeability to vanadium and enhanced H_2SO_4 absorption capability for use in vanadium redox flow batteries. *J. Mater. Chem. A* **2016**, *4*, 14342−14355.
(28) Ren, X. R.; Zhao, L. N.; Che, X. F.; Cai, Y. Y.; Li, Y. Q.; Li, H. H.; Chen, H.; He, H. X.; Liu, J. G.; Yang, J. S. Quaternary ammonium groups grafted polybenzimidazole membranes for vanadium redox flow battery applications. *J. Power Sources* **2020**, *457*, 228037.
(29) Wang, Z. Y.; Ren, J. Y.; Wan, Y. H.; Fan, X. Z.; Zhao, T. S. A secondary-doped polybenzimidazole membrane with high proton conductivity and ion selectivity for vanadium redox flow batteries. *J. Electrochem. Soc.* **2022**, *169*, 110545.

(30) Peng, S. S.; Yan, X. M.; Zhang, D. S.; Wu, X. M.; Luo, Y. L.; He, G. H. A H_3PO_4 preswelling strategy to enhance the proton conductivity of a H_2SO_4-doped polybenzimidazole membrane for vanadium flow batteries. *RSC Adv.* **2016**, *6*, 23479−23488.
(31) Noha, C.; Serhiichuk, D.; Malikah, N.; Kwon, Y.; Henkensmeier, D. Optimizing the performance of meta-polybenzimidazole membranes in vanadium redox flow batteries by adding an alkaline pre-swelling step. *Chem. Eng. J.* **2021**, *407*, 126574.
(32) Ikhsan, M. M.; Abbas, S.; Do, X. H.; Choi, X.-Y.; Azizi, K.; Hjuler, H. A.; Jang, J. H.; Ha, H. Y.; Henkensmeier, D. Polybenzimidazole membranes for vanadium redox flow batteries: Effect of sulfuric acid doping conditions. *Chem. Eng. J.* **2022**, *435*, 134902.
(33) Zhang, Q.; Dong, Q. F.; Zheng, M. S.; Tian, Z. W. The preparation of a novel anion-exchange membrane and its application in all-vanadium redox batteries. *J. Membr. Sci.* **2012**, *421*, 232−237.
(34) Wu, C.; Lu, S.; Wang, H.; Xu, X.; Peng, S.; Tan, Q.; Xiang, Y. A novel polysulfone-polyvinylpyrrolidone membrane with superior proton-to-vanadium ion selectivity for vanadium redox flow batteries. *J. Mater. Chem. A* **2016**, *4*, 1174−1179.
(35) Mu, T.; Leng, S. F.; Tang, W. Q.; Shi, N.; Wang, G. R.; Yang, J. S. High-performance and low-cost membranes based on poly(vinylpyrrolidone) and cardo-poly(etherketone) blends for vanadium redox flow battery applications. *Batteries-Basel.* **2022**, *8*, 230.
(36) Tang, W. Q.; Leng, S. F.; Jin, Y. P.; Liu, R. H.; Che, X. F.; Liu, J. G.; Yang, J. S. New crosslinked membranes based on cardo-poly(etherketone) and poly(ethylene imine) for the vanadium redox flow battery. *Eur. Polym. J.* **2021**, *161*, 110858.
(37) Tang, W. Q.; Mu, T.; Che, X. F.; Dong, J. H.; Yang, J. S. Highly selective anion exchange membrane based on quaternized poly(triphenyl piperidine) for the vanadium redox flow battery. *ACS Sustainable Chem. Eng.* **2021**, *9*, 14297−14306.
(38) Che, X. F.; Tang, W. Q.; Dong, J. H.; Aili, D.; Yang, J. S. Anion exchange membranes based on long side-chain quaternary ammonium-functionalized poly(arylene piperidinium)s for vanadium redox flow batteries. *Sci. China Mater.* **2022**, *65*, 683−694.
(39) Zhao, B. J.; Zhang, Z. J.; Zhang, J. W.; Wang, L.; Wang, T. T.; Dong, J. H.; Xu, C. X.; Yang, J. S. Long side-chain N-heterocyclic cation based ionic liquid grafted poly(terphenyl piperidinium) membranes for anion exchange membrane fuel cell applications. *Polymer* **2023**, *286*, 126404.
(40) Che, X. F.; Wang, L. L.; Wang, T.; Dong, J. H.; Yang, J. S. The effect of grafted alkyl side chains on the properties of poly(terphenyl piperidinium) based high temperature proton exchange membranes. *Ind. Chem. Mater.* **2023**, *1*, 516−525.
(41) Jin, Y. P.; Wang, T.; Che, X. F.; Dong, J. H.; Li, Q. F.; Yang, J. S. Poly(arylene pyridine)s: new alternative materials for high temperature polymer electrolyte fuel cells. *J. Power Sources* **2022**, *526*, 231131.
(42) Lv, R. X.; Jin, S.; Li, L.; Wang, Q.; Wang, L. L.; Wang, J.; Yang, J. S. The influence of comonomer structure on properties of poly(aromatic pyridine) copolymer membranes for HT-PEMFCs. *J. Membr. Sci.* **2024**, *701*, 122703.
(43) Mu, T.; Tang, W. Q.; Shi, N.; Wang, G. R.; Wang, T. T.; Wang, T.; Yang, J. S. Novel ether-free membranes based on poly(p-terphenylene methylimidazole) for vanadium redox flow battery applications. *J. Membr. Sci.* **2022**, *659*, 120793.
(44) Shi, N.; Wang, G. R.; Wang, Q.; Wang, L. L.; Li, Q. F.; Yang, J. S. Acid doped branched poly(biphenyl pyridine) membranes for high temperature proton exchange membrane fuel cells and vanadium redox flow batteries. *Chem. Eng. J.* **2024**, *489*, 151121.
(45) Chen, N. J.; Wang, H. H.; Kim, S. P.; Kim, H. M.; Lee, W. H.; Hu, C.; Bae, J. Y.; Sim, E. S.; Chung, Y.-C.; Jang, J.-H.; Yoo, S. J.; et al. Poly (fluorenyl aryl piperidinium) membranes and ionomers for anion exchange membrane fuel cells. *Nat. Commun.* **2021**, *12* (1), 2367.
(46) Popelier, P. L. A.; Maxwell, P. I.; Thacker, J. C. R.; Alkorta, I. A relative energy gradient (REG) study of the planar and perpendicular torsional energy barriers in biphenyl.Theor. *Chem. Acc.* **2019**, *138* (1), 12.
(47) Lim, H.; Jeong, J.-Y.; Lee, D. H.; Myeong, S.-W.; Shin, G.; Choi, D.; Kim, W. B.; Choi, S. M.; Park, T. Morphology and cell performance of poly (fluorene)-based anion exchange membranes for water electrolysis: effect of backbone core structure.J. *J. Mater. Chem. A* **2023**, *11* (47), 25938−25944.
(48) Dong, T. V.; Tinh, V. D. C.; Kim, D. Ether-free sulfonated poly (fluorene biphenyl indole) membranes and ionomer binders for proton exchange membrane fuel cells.J. *Power Sources* **2023**, *556*, 232418.
(49) Gonzalez-Díaz, M. O.; Cetina-Mancilla, E.; Sulub-Sulub, R.; Montes-Luna, A.; Olvera, L. I.; Zolotukhin, M. G.; Cardenas, J.; Aguilar-Vega, M. Novel fluorinated aromatic polymers with ether-bond-free aryl backbones for pure and mixed gas separation. *J. Membr. Sci.* **2020**, *606*, 118114.
(50) Tan, J. H.; Wang, Q.; Liu, Y. W.; Zeng, Y.; Ding, Q.; Wu, R. M.; Liu, Y. J.; Xiang, X. W. Synthesis, gas barrier and thermal properties of polyimide containing rigid planar fluorene moieties.J. *Macromolecular Sci. Part A* **2018**, *55*, 75−84.
(51) Ikhsan, M. M.; Abbas, S.; Do, X. H.; Ha, H. Y.; Ha, H. Y.; Azizi, K.; Henkensmeier, D. Sulfonated polystyrene/polybenzimidazole bilayer membranes for vanadium redox flow batteries. *Adv. Energy Mater.* **2024**, 2400139.
(52) Pang, B.; Du, R. H.; Chen, W. T.; Cui, F.; Wang, N.; Zhao, H. M.; Wu, X. M.; Tiantian, L.; He, G.; Wu, X. Self-supporting sulfonated covalent organic framework as a highly selective continuous membrane for vanadium flow battery. *Energy Storage Mater.* **2024**, *67*, 103293.
(53) Tang, W. Q.; Yang, Y. F.; Liu, X. L.; Dong, J. H.; Li, H. H.; Yang, J. S. Long side-chain quaternary ammonium group functionalized polybenzimidazole based anion exchange membranes and their applications. *Electrochim. Acta* **2021**, *391*, 138919.
(54) Bui, T. T.; Shin, M.; Abbas, S.; Ikhsan, M. M.; Do, X. H.; Dayan, A.; Almind, M. R.; Park, S.; Aili, D.; Hjelm, J.; Hwang, J.; et al. Sulfonated para-polybenzimidazole membranes for use in vanadium redox flow batteries. *Adv. Energy Mater.* **2024**, 2401375.
(55) Zhang, Y.; Liu, H.; Liu, M.; Ma, X.; Liang, D.; Qian, P.; Yan, J. Highly ion selective sulfonated poly (ether ether ketone)/polyzwitterion functionalized graphene oxides hybrid membrane for vanadium redox flow battery. *Int. J. Hydrogen Energy* **2024**, *53*, 229−238.

https://doi.org/10.1021/acsapm.4c03945
ACS Appl. Polym. Mater. XXXX, XXX, XXX−XXX